Original

Carpenter, J.R.; Guha, A.; Heifetz, E.:

A Physical Interpretation of the Wind-Wave Instability as Interacting Waves

Journal of Physical Oceanography (2017) AMS

DOI: 10.1175/JPO-D-16-0206.1

A Physical Interpretation of the Wind-Wave Instability as Interacting Waves

J. R. CARPENTER

Institute of Coastal Research, Helmholtz-Zentrum Geesthacht, Geesthacht, Germany

A. GUHA

Department of Mechanical Engineering, Indian Institute of Technology Kanpur, Kanpur, India

E. HEIFETZ

Department of Geosciences, Tel Aviv University, Tel Aviv, Israel

(Manuscript received 8 September 2016, in final form 24 February 2017)

ABSTRACT

One mechanism for the growth of ocean surface waves by wind is through a shear instability that was first described by Miles in 1957. A physical interpretation of this wind-wave instability is provided in terms of the interaction of the surface gravity wave with perturbations of vorticity within the critical layer—a near-singularity in the airflow where the background flow speed matches that of the surface gravity wave. This physical interpretation relies on the fact that the vertical velocity field is slowly varying across the critical layer, whereas both the displacement and vorticity fields vary rapidly. Realizing this allows for the construction of a physically intuitive description of the critical layer vorticity perturbations that may be approximated by a simple vortex sheet model, the essence of the wind-wave instability can then be captured through the interaction of the critical layer vorticity with the surface gravity wave. This simple model is then extended to account for vorticity perturbations in the airflow profile outside of the critical layer and is found to lead to an exact description of the linear stability problem that is also computationally efficient. The interpretation allows, in general, for the incorporation of sheared critical layers into the ''wave interaction theory'' that is commonly used to provide a physical description and rationalization of results in the stability of stratified shear flows.

1. Introduction

Here we are concerned with understanding the growth of water waves from the presence of a sheared airflow above. This is a classic problem in fluid mechanics, with contributions from many authors (e.g., Jeffreys 1925; Miles 1957; Phillips 1957; Belcher and Hunt 1993). One of the foremost solutions is that found by Miles (1957) using a linear stability analysis (see also Lighthill 1962). In his paper, Miles made the essential realization that instability arises through the formation of a near-singularity in the airflow. This near-singularity occurs within a thin ''critical layer'' centered at the critical height, the vertical location where the background flow speed matches the surface gravity wave speed. Since Miles' analysis, much has been learned about the critical layer, and it has been studied in many different contexts in geophysical fluid dynamics (see, e.g., Bühler 2009).

Despite decades of research, there is currently no consensus in the literature on the underlying mechanism responsible for the wind-induced growth of surface waves (Sullivan and McWilliams 2010). Two principal competing theories have arisen: the Miles (1957) critical layer mechanism and the so-called nonseparated sheltering mechanism based on the work of Belcher and Hunt (1993, 1998). Both of these theories have received experimental support and could be relevant depending on the parameter regime; however, we choose to focus on the critical layer theory of Miles (1957). Recent observational evidence of the presence of a critical layer in the airflow above ocean waves has also been found by Hristov et al. (2003) and Grare et al. (2013). In addition, controlled laboratory experiments by Buckley and Veron (2016) demonstrate the presence of a critical

Corresponding author: J. R. Carpenter, jeff.carpenter@hzg.de

DOI: 10.1175/JPO-D-16-0206.1

layer, despite the presence of a highly turbulent airflow, in agreement with the predictions of Miles' theory. In all of these observations, the critical layer only emerges once significant phase averaging of the airflow over the waves is accomplished, hinting at the difficulties in directly observing the critical layer dynamics.

The wind-wave instability is a special instance of the stability of stratified shear flows, and one should expect that the basic principles governing these flows may be used to understand the wind-wave instability. One method that has been used to understand instability in stratified shear flows is wave interaction theory (WIT; see the review by Carpenter et al. 2013, and references therein). In this theory, instability results from the interaction of two fundamental wave types: (i) vorticity waves that propagate along vertical gradients of vorticity (also referred to as counterpropagating Rossby waves and Rayleigh waves) and (ii) gravity waves that propagate along vertical density gradients. The WIT leads naturally to a physical understanding of the famous Rayleigh and Fjørtoft conditions, which can be understood in terms of interacting vorticity waves, as well as explaining the sometimes destabilizing role of density stratification (Baines and Mitsudera 1994; Caulfield 1994; Rabinovich et al. 2011; Carpenter et al. 2013).

Our physical interpretation of the wind-wave instability put forward in this paper can be considered complimentary to that discussed in Lighthill (1962), but the details differ considerably. Lighthill's classic interpretation, in his own words, is aimed "at showing how a vertical velocity fluctuation at the critical layer (with non-zero amplitude) generates a concentrated vortex force, retarding the fluid in the layer, and making it give up energy and momentum to the water waves." His physical interpretation is formulated in terms of vortex force, pressure, vertical velocity, energy, and momentum and has become the standard basis for explanations of the critical layer view of wave growth in texts on wind-generated ocean waves (e.g., Kinsman 1965; Janssen 2004). In contrast, our physical interpretation uses the quantities of displacement, vorticity, and vertical velocity to explain the instability and the structure of the critical layer in what we feel are the simplest possible terms. Note also that these are the only ingredients required in the derivation of Rayleigh's equation, which is essentially what governs the airflow dynamics of the instability. This description is very different, but complimentary to Lighthill's: our primary objective is to develop a simple (kinematic) model and description for the vorticity structure of the critical layer and show how this creates a feedback with the water wave to produce instability.

In this paper we show that the critical layer can be accounted for in a straight-forward manner that fits nicely into the WIT; essentially, the critical layer is modeled as another type of interface, just as the vorticity and density interfaces that support the propagation of vorticity and gravity waves. We also show that this can be used to generate a good approximation to the wind-wave instability by considering only the very simple case of a critical layer interacting with a surface gravity wave. This simple approximation not only leads to an analytical form for the growth rate that can easily be used for any velocity profile, but also to a "minimal" model needed to explain the essential instability. Understanding shear instabilities in terms of two interacting waves is the great advantage of WIT and leads to a simple physical interpretation of the instability. We show that the differences between this minimal model prediction of the growth rate and the full solution can be attributed to the influence of the vorticity perturbations in the airflow outside the critical layer. This can easily be accounted for, however, by including vorticity interfaces in the airflow by representing the velocity profile by a piecewise-linear curve. The WIT can then offer a physical explanation of these airflow contributions outside the critical layer.

The paper is organized as follows. After reviewing the relevant mathematical background (section 2), we discuss a simple physical description of the continuous structure of the critical layer. This structure is then used to formulate an "interfacial," or vortex sheet, representation of the critical layer that is used in section 4 to create a minimal model of the wind-wave instability. The minimal model is then extended in section 5 to include any number of vorticity interfaces in order to account for vorticity perturbations in the airflow outside the critical layer, leading to an exact, and numerically efficient, description of the linear instability. In the final two sections we discuss the limitations of the minimal model and summarize our physical interpretation in the context of WIT.

2. Background

a. Formulation of the wind-wave problem

The evolution of small amplitude perturbations in a stratified shear flow characterized by a background density profile $\overline{\rho}(z)$ and horizontal velocity profile $U(z)$ may be found by linearizing the equations of motion about this background and searching for normal mode solutions for the perturbation vertical velocity of the form $\tilde{w}(x, z, t) = w(z)e^{ik(x-ct)}$. This results in an eigenvalue problem that is governed by the following

equation (see Janssen 2004, section 3.1, with different notation):

$$\{\overline{\rho}[(U-c)w' - U'w]\}' - \frac{\overline{\rho}'g}{U-c}w - \overline{\rho}(U-c)k^2w = 0, \tag{1}$$

for the eigenvalue $c = c_r + ic_i$, giving both the wave phase speed c_r and the growth rate ($\sigma \equiv kc_i$), as well as the eigenfunction $w(z)$ describing the vertical structure of the mode. Here we have used k to denote the horizontal wavenumber of the perturbation, g is the gravitational acceleration in the negative z direction, and the primes indicate ordinary differentiation with respect to z. Note that this is the non-Boussinesq form of the well-known Taylor–Goldstein equation, which can be recovered by taking $\overline{\rho}(z) = \rho_0$ a constant, while $\overline{\rho}'$ remains a function of z.

For the wind-wave instability we look at the case of background profiles in an unbounded domain, with a sheared airflow at $z > 0$, over a stationary water layer for $z < 0$, so that

$$\overline{\rho}(z) = \begin{cases} \rho_a, & z > 0 \\ \rho_w, & z < 0 \end{cases} \quad \text{with} \quad \overline{\rho}'(z) = -\Delta\rho\delta(z), \tag{2}$$

where ρ_a and ρ_w are the air and water densities, respectively, and $\Delta\rho \equiv \rho_w - \rho_a$. The velocity profile is also taken such that $U = 0$ in the water. This leads to the simplified form of

$$w'' - k^2w = 0 \tag{3}$$

in the water ($z < 0$), implying $w(z) \propto e^{kz}$ given the boundary condition that $w \to 0$ as $z \to -\infty$. In the air ($z > 0$), we must solve Rayleigh's equation

$$w'' - \left(k^2 + \frac{U''}{U-c}\right)w = 0, \tag{4}$$

where we have assumed that $\mathrm{Im}(c) = c_i \neq 0$ so that a vanishing $U - c_r$ does not lead to a singular term.

In effect, we have split the problem into one for each of the air and water layers. However, they are coupled through a "jump" condition at the air–water interface. This condition is found by integrating (1) across $z = 0$ to give

$$[\![\overline{\rho}[(U-c)w' - U'w]]\!]_s + \frac{\Delta\rho g}{U_s - c}w_s = 0, \tag{5}$$

where the s subscript refers to quantities evaluated at the water surface ($z = 0$) and $[\![f]\!]_z = [f]_{z^-}^{z^+}$ denotes the jump in f at z.

Suppose that $U(z)$ monotonically approaches some maximum value U_∞. We can then define a length scale by $h = U_\infty/U'(0^+)$ and nondimensionalize with respect to U_∞, ρ_w, and h, with the following new variables:

$$w = U_\infty w_*, \quad U = U_\infty U_*, \quad c = U_\infty c_*, \quad z = hz_*, \quad k_* = kh. \tag{6}$$

Dropping the asterisks and working henceforth with dimensionless quantities unless otherwise noted leads to Rayleigh's equation in the air in the exact same form as above and a jump condition at the interface of

$$[\![\overline{\rho}[(U-c)w' - U'w]]\!]_s + (1-r)m\frac{w_s}{U_s - c} = 0, \tag{7}$$

in general. Once the dimensionless profiles are substituted this jump condition can be simplified to

$$(k - r\Xi)c^2 - rc - (1-r)m = 0. \tag{8}$$

Here we have defined $r \equiv \rho_a/\rho_w$ as the density ratio, $m \equiv gh/U_\infty^2$, $\Xi \equiv w_+'/w_s$, and use the notation that $f_\pm \equiv f(0^\pm)$. It is important to note that we consider only background velocity profiles $U(z)$ that are continuous. They exhibit no jumps that would lead to the presence of vortex sheets in the mean flow $U(z)$. The Kelvin–Helmholtz instability arising from a vortex sheet in $U(z)$ is therefore not considered in this paper. These modes could easily be included by appropriate substitution into (7), as described by, for example, Alexakis et al. (2002).

Together with the boundary condition $w \to 0$ as $z \to \infty$, (4) and (8) define the problem to be solved.

b. *Miles' approximation*

In Miles' original paper, he simplified the problem by writing the solution as an asymptotic expansion in terms of the small quantity $r = O(10^{-3})$. Following Young and Wolfe (2014), this is done first by writing (8) as

$$D(c,k) \equiv D_0(c,k) + rD_1(c,k) = 0, \tag{9}$$

and seeking approximate solutions of the form

$$c(k,r) = c_0(k) + rc_1(k) + \cdots, \tag{10}$$

we find that to zeroth order in r we get

$$D_0(c,k) = 0 \quad \Rightarrow \quad c_0 = \left(\frac{m}{k}\right)^{1/2}, \tag{11}$$

that is, the dispersion relation for a deep-water gravity wave in the absence of a sheared airflow. Now, expanding the dispersion relation about $c = c_0$,

$$D = D(c_0, k) + (c - c_0)\left.\frac{\partial D}{\partial c}\right|_{c=c_0} \tag{12}$$

$$= rD_1(c_0, k) + rc_1\partial_c D_0|_{c=c_0} = 0 \tag{13}$$

and this results in the following approximation for c_1:

$$c_1 = -\frac{D_1(c_0, k)}{\partial_c D_0(c_0, k)}. \tag{14}$$

Substituting in $D_1(c_0, k) = -\Xi(c_0, k)c_0^2 - c_0$ and $\partial_c D_0(c_0, k) = 2kc_0$ gives

$$c = c_0 + r\left\{\frac{1}{2k} + \frac{c_0}{2}\left[\frac{\Xi(c_0, k)}{k} - 1\right]\right\} \tag{15}$$

to order r.

There are a couple of things to note in this equation. First, if we neglect any contribution of the airflow curvature (U'') above the surface and consider only the rightward propagation of neutral waves on the air–water interface, $\Xi = -k$ and $c = (1 - r)c_0 + r/2k$. The first term $[(1 - r)c_0]$ represents changes to the deep water wave speed due to non-Boussinesq effects, and the second $(r/2k)$ represents the contribution of the vorticity wave at the kink in $U(z)$ at the air–water interface (Heifetz and Mak 2015). Therefore, any deviations of the real part of Ξ from $-k$ when the airflow curvature is included will lead to slight changes in the phase speed of the surface wave. Additionally, Ξ may have an imaginary part, which leads to an approximation for the growth rate

$$\sigma \equiv k\,\mathrm{Im}(c_1) = \frac{rc_0}{2}\mathrm{Im}[\Xi(c_0, k)]. \tag{16}$$

Also, Ξ can be found by integrating Rayleigh's equation directly, since it is evaluated at $c = c_0$. In Miles' original paper he goes on to describe an ad hoc approximation for Ξ that we shall not consider in the following. Instead, we examine other solution approaches.

c. An exact solution using Miles' approximation

Focusing on the special case of a wind profile that is represented by the exponential form

$$U(z) = 1 - e^{-z}, \quad \text{for} \quad z > 0, \tag{17}$$

Rayleigh's equation can be transformed into a hypergeometric equation. An analytical solution is therefore possible, and this has been found by Hughes and Reid (1965) [see also Miles' solution in Morland and Saffman (1993), and Young and Wolfe (2014)] with

$$w(z) = e^{-kz}f(\tau), \quad f(\tau) = \frac{F(a, b; s; \tau)}{F_0}, \quad \text{and}$$

$$\tau \equiv \frac{e^{-z}}{1 - c}, \tag{18}$$

where $F_0 \equiv F(a, b, s; z = 0, a \equiv k + (1 + k^2)^{1/2}, b \equiv k - (1 + k^2)^{1/2}, s \equiv 1 + 2k$, and F is the Gaussian hypergeometric function. The growth rates may be found by solving for the quantity Ξ, which is given by

$$\Xi(c, k) = -k + \frac{1}{(1 + 2k)(1 - c)} \times \frac{F(a + 1, b + 1, s + 1; z = 0)}{F(a, b, s; z = 0)}, \tag{19}$$

where a differentiation identity has been used for the hypergeometric function [see Young and Wolfe (2014) for more details].

3. A model of the critical layer

In this section we formulate a simple model of the structure within the critical layer of three important fields: the vertical velocity w, vertical displacement of material lines η [as described by the linearized kinematic condition in (21) below], and the vorticity $\tilde{q} \equiv \partial\tilde{u}/\partial z - \partial\tilde{w}/\partial x$. Throughout the paper, tildes indicate that the variable is a function of the (x, z, t) coordinates, and with the tilde dropped indicates an eigenfunction dependent only on height z. All three of these fundamental fields (w, η, q) are closely related, and their interaction forms the basis of the wave interaction perspective on shear instabilities (Harnik et al. 2008; Carpenter et al. 2013).

The key to formulating our model is to realize that in the critical layer both η and q vary rapidly with the small characteristic length scale δ_c (to be defined precisely later on), while w is gradually varying with the characteristic length scale k^{-1}. This can be seen by relating w and q through the following vorticity inversion formula

$$L[w] \equiv \frac{i}{k}\left(\frac{d^2}{dz^2} - k^2\right)w = q(z) \quad \Rightarrow$$

$$w(z) = \int_{-\infty}^{+\infty} G(s, z)q(s)\,ds, \tag{20}$$

where Green's function $G(s, z) = ie^{-k|z-s|}/2$ for the differential operator L, in an unbounded vertical domain (see Harnik et al. 2008; Carpenter et al. 2010). The effect of Green's function spreads any abrupt q variation over a length scale k^{-1}. This can easily be seen through a simple example by taking an infinitely

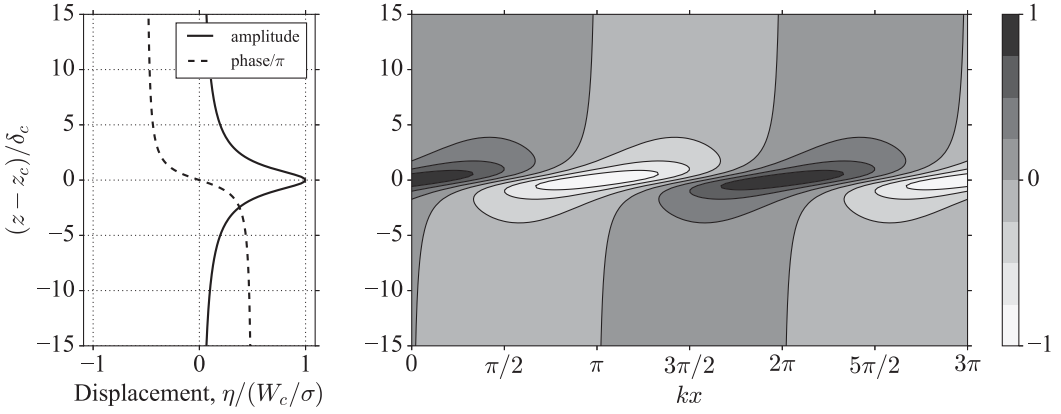

FIG. 1. The braided structure of the model critical layer. (left) The displacement η normalized by W_c/σ is plotted, but the vorticity q normalized by $W_c U_c''/\sigma$ is identical apart from a change in sign. (right) The vertical velocity field applied at the critical layer has crests (maximum upward w) at $kx = 0, 2\pi$ and troughs (maximum downward w) at $kx = \pi, 3\pi$.

abrupt delta function vorticity, that is, $q(z) = \delta(z)$. Then the vertical velocity produced is simply $w(z) = (i/2)e^{-k|z|}$, which decays away from the vorticity spike over a distance k^{-1}.

a. *Vertical displacement structure*

Now consider the perturbation of the vertical displacement field of material lines that are horizontal in the undisturbed airflow. Using the linearized kinematic condition for the motion of these material lines, we can write

$$\frac{\partial\tilde{\eta}}{\partial t} + U\frac{\partial\tilde{\eta}}{\partial x} = \tilde{w} \quad \Rightarrow \quad \eta = \frac{-iw}{k(U-c)}, \tag{21}$$

and formulate the response at the critical layer to a vertical velocity incident upon it. This velocity will be due to both the surface gravity wave influence as well as any disturbances in the airflow.[1] We give this (sinusoidal in x) vertical velocity a *constant* amplitude of W_c *throughout* the critical layer, since it is slowly varying in the vertical in comparison to the critical layer width. Continuing with this approximation, we can write $U - c \approx U_c'(z - z_c) - ic_i$ and $U'' \approx U_c''$ for $z \approx z_c$. Then the vertical displacement near the critical layer is given by

$$\eta \approx \frac{-iW_c}{kU_c'(z-z_c) - i\sigma}, \tag{22}$$

which is plotted in Fig. 1. It is important to note that the critical layer is not singular because $\sigma > 0$ for unstable flows. Equation (22) shows that η reaches a maximum at z_c of W_c/σ, with an amplitude that decays as $(z - z_c)^{-1}$, and a phase change of π radians across z_c. Since σ is a small quantity (of order r), however, the critical layer displacements are large, and we therefore refer to it as a near-singularity.

The "braided" displacement structure at the critical layer shown in Fig. 1 can be understood as resulting from (i) unsteady growth and (ii) advection of displacement gradients, which alternate in balancing the vertical velocity—essentially a source term for vertical displacements. Rewriting (22) as

$$\sigma\eta + ikU_c'(z - z_c)\eta = W_c, \tag{23}$$

shows that the first term represents unsteady growth, the second term represent advection of horizontal η gradients, and the right-hand side represents the production/destruction of η (i.e., a forcing term). Directly at the critical layer there is no horizontal advection of displacements, so W_c is acting directly to increase η (Fig. 2). This produces a displacement that is in phase with W_c, with the exact value being $\eta = W_c/\sigma$. As the distance from z_c increases, we find an increasing advection of the vertical displacement field past the W_c field that is providing the forcing. The sinusoidal displacements at height z then experience a forcing at the frequency $kU_c'(z - z_c)$, and the amplitude of any displacements will periodically grow and decay at this frequency. In this case, where advection is dominant, η will have a maximum and minimum amplitude that are $\pm\pi/2$ radians out of phase with the forcing, depending on the

[1] In fact, this vertical velocity includes all airflow disturbances, including that from the critical layer itself. It must be determined as part of the solution, and this is described and carried out in sections 4 and 5.

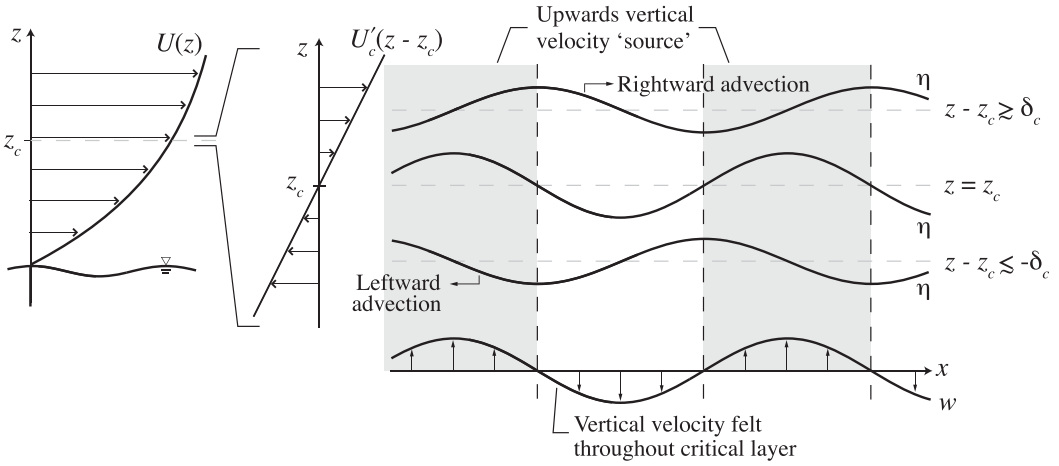

FIG. 2. Sketch of the processes setting the displacement structure of the critical layer.

direction of the advection, that is, the sign of $U_c'(z - z_c)$. The phase shift results because the maximum positive (negative) displacements occur after experiencing a full half-cycle of upward (downward) vertical velocity (see Fig. 2). This leads to the rapid phase shift of π radians across the critical layer and the characteristic braided structure of Fig. 1.

The transition between whether unsteady growth or advection is dominant on the left-hand side of (23) depends on the ratio of these two terms, $k|U_c'(z - z_c)|/\sigma$, and leads naturally to a measure of the width of the critical layer,

$$\delta_c \equiv \frac{\sigma}{k|U_c'|}. \tag{24}$$

This length scale characterizes the region of the critical layer where an appreciable phase change in η occurs and has been used to nondimensionalize z in Fig. 1. Note that the ratio of the critical layer width, to the length scale of variations in w, is $\varepsilon \equiv k\delta_c = \sigma/|U_c'| \ll 1$ for the wind-wave instability. However, when other processes that are relevant for ocean wave generation by wind are included, such as viscosity and nonlinearity, it is generally these processes that set the thickness of the critical layer. Although much work has been carried out on the nonlinear dynamics of critical layers (Maslowe 1986; Alexakis et al. 2004a,b) we have chosen to limit the scope of this paper to the linear inviscid regime.

Now that the displacement field in the region of the critical layer is known, it is a simple matter to construct the perturbation vorticity field $q = i(w'' - k^2 w)/k$. Within the linear approximation, q results simply from the vertical displacement of the background vorticity gradients, that is, $q = -U_c''\eta$. Therefore, the vorticity perturbation in the critical layer is identical to η except for a sign change, when normalized by $W_c U_c''/\sigma$, as shown in Fig. 1. Mathematically, this is written as

$$q \approx \frac{iU_c'' W_c}{kU_c'(z - z_c) - i\sigma}. \tag{25}$$

b. Vertical velocity structure

Given our model predictions for the q structure at the critical layer, we can now use this to find the w that this produces. In other words, we now calculate the vertical velocity response of the critical layer to a vertical velocity incident upon it. This is done by multiplying (25) by k/i and using the inversion property from (20). For our model critical layer q distribution we can therefore write

$$w(z) \approx -\frac{U_c'' W_c}{2kU_c'} \int_{y_c^-}^{y_c^+} \frac{e^{-|y-s|}}{s - y_0} ds, \tag{26}$$

where $y \equiv kz$ and $y_c^{\pm} \equiv kz_c^{\pm}$ are the integration boundaries and $y_0 \equiv kz + i\varepsilon$ is the location of the singularity in the complex k–z plane. The integration boundaries have been chosen as finite since our approximation for q is valid only locally around the critical layer. After some algebra, this integral can be expressed in terms of the generalized incomplete gamma function

$$\Gamma(n, a, b) \equiv \int_a^b \zeta^{n-1} e^{-\zeta} d\zeta, \tag{27}$$

as

$$K(y,y_0,y_c^{\pm}) \equiv \begin{cases} e^{y_0-y}\Gamma(0,y_0-y_c^-,y_0-y_c^+), & y>y_c^+ \\ e^{y_0-y}\Gamma(0,y_0-y_c^-,y_0-y)+e^{y-y_0}\Gamma(0,y-y_0,y_c^+-y_0), & y_c^-<y<y_c^+ \\ e^{y-y_0}\Gamma(0,y_c^--y_0,y_c^+-y_0), & y<y_c^- \end{cases} \tag{28}$$

with the vertical velocity given by

$$w(z) = -\beta_c W_c K(kz,y_0,y_c^{\pm}), \tag{29}$$

where $\beta_c \equiv U_c''/2kU_c'$.

We now examine the w structure at the critical layer in the case where the integration limits in (26) are taken such that $\varepsilon \ll y_c^+ - y_c^- \ll k^{-1}$. In other words, we integrate across the critical layer q distribution (i.e., a scale large compared with δ_c), but over a scale that is small relative to k^{-1}, so that w can be considered constant. In this case, we see that

$$w(z) \approx -i\pi\beta_c W_c e^{-k|z-z_c|} \tag{30}$$

either by direct evaluation of $K(y, y_0, y_c^{\pm})$ or by approximation of the integral in (26) by

$$\int_{y_c^-}^{y_c^+} \frac{e^{-|y-s|}}{s-y_0}\,ds \approx e^{-k|z-z_c|}\int_{y_c^-}^{y_c^+}\frac{ds}{s-y_0} \approx -i\pi e^{-k|z-z_c|}, \tag{31}$$

from the slowly varying assumption ($y_c^+ - y_c^- \ll k^{-1}$), and by ensuring the entire critical layer is captured in the integration ($y_c^+ - y_c^- \gg \varepsilon$). This shows that the local critical layer response to the vertical velocity of the surface gravity wave is a w that is $\pi/2$ out of phase with an amplitude that is $\pi\beta_c$ times greater than the value incident on it. (The case where the integration limits are large is treated in the appendix.)

This ''local'' representation of the critical layer is a type of vortex sheet approximation for perturbations at the critical layer. The value of $\int(s-y_0)^{-1}\,ds$ may be thought of as being related to the strength of an equivalent vortex sheet (circulation per unit length) located at the critical layer that produces the vertical velocity field in (30). The sheet strength is given by

$$[\![u]\!]_c \equiv \int_{z_c^-}^{z_c^+} q(z)\,dz = 2i\beta_c W_c \int_{y_c^-}^{y_c^+}\frac{ds}{s-y_0} = -2\pi\beta_c W_c, \tag{32}$$

and is therefore in phase with W_c, as expected from the simple relation $q = -U''\eta$ (recall that $\beta_c < 0$). Note that since the sheet strength is a part of the perturbation field, it is also sinusoidal in x.

The use of vortex sheets for modeling shear instabilities had its beginnings with the piecewise-constant (layered) velocity profile of Kelvin (1871). He showed that the sheet was unstable to sinusoidal perturbations of all wavenumbers, through a physical mechanism causing the concentration of vorticity through self-advection as described in Drazin and Reid (1982, p.15), for example. In wave interaction theory, the dynamics of vorticity and density interfaces are also represented by vortex sheets but whose strength depends on the interfacial displacement: for a vorticity interface, the sheet strength is directly proportional to the displacement, whereas for a density interface the time rate of change of the sheet strength is proportional to the slope of the displacement (Redekopp 2001). These sheets arise in the perturbation fields, opposed to the mean flow $U(z)$, and are therefore sinusoidal in x. In isolation, the vortex sheet interfaces lead to stable wave propagation, and only through their interaction can instability arise, in contrast to the vortex sheet present in the piecewise-constant velocity profile exhibiting Kelvin–Helmholtz instability (Carpenter et al. 2013). We have just shown that the critical layer sheet strength (part of the perturbation field) is instead dependent on the vertical velocity incident on it (W_c). It cannot exist in isolation, because its construction was based on a nonzero growth rate, and this can only result from the presence of an externally applied w field from some other distant vorticity source.

4. A minimal wave interaction view of wind-wave growth

Using our solution for the vertical velocity induced at the critical layer by an incident velocity perturbation W_c found in the last section, we proceed to create a ''minimal model'' of the wind-wave instability. This is done by treating the critical layer as another type of interface (i.e., a sinusoidally varying vortex sheet perturbation) and calculating the interaction between it and the surface gravity wave. Any other contribution of the airflow to the wave growth is ignored in this section.

Before we state the mathematical solution to this minimal model, it is useful to describe in words the essentials of the interaction and how it leads to wind-wave growth as sketched in the wave-field diagram of Fig. 3. The propagation of the surface gravity wave generates a w field that is $\pi/2$ radians out of phase with the surface

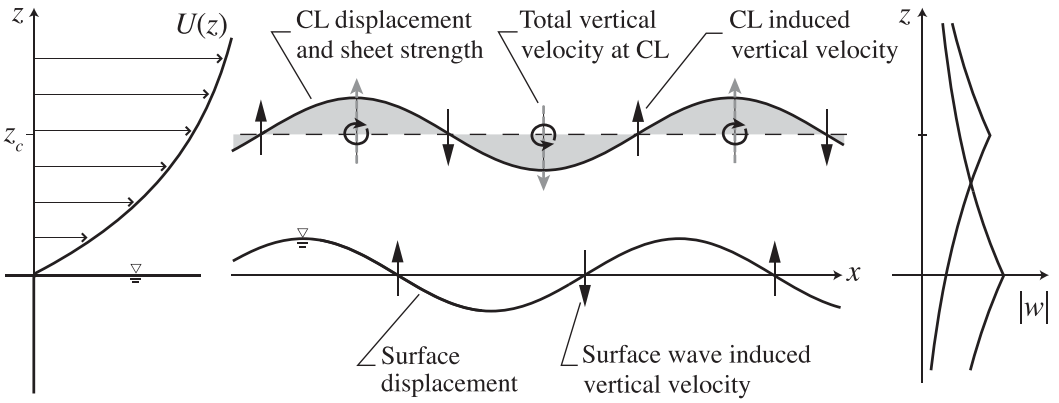

FIG. 3. Wave field diagram of the critical layer–gravity wave interaction in the minimal model of the wind-wave instability.

displacement. This is a general property of stable interfacial wave propagation that occurs in the absence of interaction with the airflow and corresponds to Miles' zeroth-order solution. The w field set up in this way decays exponentially over the scale k^{-1}, perturbing the critical layer with a vertical velocity. Since the rapid phase change of the critical layer q field occurs over the extremely thin length scale $\delta_c \ll k^{-1}$, it may be considered as an infinitely thin vortex sheet with strength $(-2\pi\beta_c W_c)$ that is in phase with the total vertical velocity forcing it, W_c (since $\beta_c < 0$). This vorticity perturbation leads to an induced vertical velocity $\pi/2$ out of phase with the vertical velocity incident on the critical layer W_c. The W_c at the critical layer therefore has both a surface wave and critical layer component and is not directly in phase with the surface wave vertical velocity. Most crucial is that the vertical velocity induced at the critical layer has a component that is in phase with the surface wave displacement. Then, as shown in Fig. 3, the vertical velocity fields induced at both the water surface and the critical layer cause a mutual growth in the displacement field of each other, increasing the strength of both vorticity and vertical velocity perturbations. This provides the positive feedback mechanism that is the basis of the wave interaction theory of shear instabilities (Carpenter et al. 2013).

Mathematically, the perturbation vorticity field is composed of two "interfaces" that are modeled as vortex sheets, that is,

$$q(z) = \hat{q}_s \delta(z) + \hat{q}_c \delta(z - z_c), \tag{33}$$

with sheet strengths of $\hat{q}_s$ at the surface, and $\hat{q}_c$ at the critical layer. The total w can therefore be written using (20) as

$$w(z) = \frac{i}{2}(\hat{q}_s e^{-k|z|} + \hat{q}_c e^{-k|z-z_c|}). \tag{34}$$

The coefficient of the critical layer term is given from (32) as $\hat{q}_c = -2\pi\beta_c W_c$. Substituting this back into (34) and evaluating the expression at z_c then gives

$$W_c = \frac{i\hat{q}_s e^{-k|z_c|}}{2} - i\pi\beta_c W_c. \tag{35}$$

This equation states that the vertical velocity at the critical layer is composed of the surface gravity wave (or, in the general case, the sum of all sources outside the critical layer) plus a component that is $\pi/2$ out of phase with it. Indeed, we have seen that the critical layer accepts an incoming vertical velocity and produces a response that is $\pi/2$ out of phase with it. This leads to an apparent contradiction since the vertical displacement and the vertical velocity must be in phase at the critical layer in order for the displacements to be stationary, that is, since $U(z_c) - c_r = 0$, we must have $\eta_c = W_c/\sigma$. However, there is a unique value of

$$W_c = \frac{i\hat{q}_s e^{-k|z_c|}}{2(1 + i\pi\beta_c)} \tag{36}$$

that is obtained by solving (35), in which the correct amplitude and phase are found in order for the total vertical velocity at the critical layer to be $\pi/2$ out of phase with the local generation of vertical velocity. This results in a phase change between the vertical velocity induced by the surface wave and the displacement at the critical layer as sketched in Fig. 3. Using this value for W_c allows us to write the solution up to an arbitrary constant, that is,

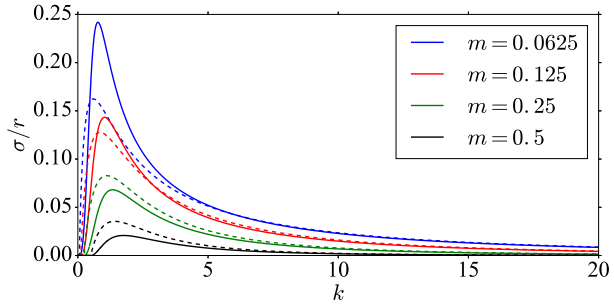

FIG. 4. Approximation to the growth rates of the wind-wave instability using the minimal model (dashed lines) consisting of a surface gravity wave interacting with the critical layer. The exact solution using Miles' approximation described by (16) and (19) and outlined in section 2c is plotted as solid lines. The exponential profile is used, and four different values of m are shown, corresponding to the different colors. The Gaussian hypergeometric function was evaluated using the "scipy" package of the Python programming environment.

$$w(z) = \frac{i\hat{q}_s}{2}\left(e^{-k|z|} - \frac{i\pi\beta_c e^{-k|z_c|}}{1+i\pi\beta_c} e^{-k|z-z_c|}\right). \quad (37)$$

Within Miles' $O(r)$ approximation, the location of the critical layer is known from $U(z_c) = c_0$, so the growth rate σ may be determined directly from $\Xi(k, c_0)$ and is found to be

$$\sigma = \frac{rc_0}{2}\mathrm{Im}(\Xi) = -\frac{rkc_0}{2}\mathrm{Im}\left[\frac{1+i\pi\beta_c(1+e^{-2k|z_c|})}{1+i\pi\beta_c(1-e^{-2k|z_c|})}\right]. \quad (38)$$

The comparison of this analytical approximation for σ in the minimal model of the wind-wave instability, to the exact solution of the exponential profile described in section 2c, is shown in Fig. 4. We see that the minimal model captures the essence of the instability, exhibiting a peak at low k and a gradual tail at larger k. For $k > 5$, the minimal model closely describes the growth rates and the modal structure $w(z)$ (not shown). However, the minimal model can both over- and underestimate the growth rates at low k around the region of the most unstable mode. In the next section we show that this is due to our neglect of perturbations in the rest of the airflow shear profile.

5. Extension to many interfaces

It is possible to extend the minimal model to account for the presence of vorticity perturbations in the airflow outside of the narrow critical layer region. This is done by adding additional vorticity interfaces, that is, vertical levels z_i, where the background vorticity (U') changes abruptly. This is equivalent to representing the velocity profile by a piecewise linear curve. In such a representation, the background vorticity gradient is represented by a sum of N delta functions

$$U''(z) = \sum_{i=0}^{N-1} \Delta Q_i \delta(z - z_i), \quad (39)$$

with amplitudes given by the vorticity jumps across each interface $\Delta Q_i \equiv [\![U']\!]_i$. The solution to Rayleigh's equation for this velocity profile can immediately be written as

$$w(z) = \sum_{i=0}^{N} \hat{q}_i G(z, z_i) = \frac{i}{2}\sum_{i=0}^{N} \hat{q}_i e^{-k|z-z_i|} \quad (40)$$

with the surface vorticity now included in the sum, and it remains to solve for the interfacial vortex sheet strengths $\hat{q}_i$. This is done by forming an equivalent vorticity conservation equation for the interfacial perturbations by integrating Rayleigh's equation across each interface. This gives the jump condition

$$(U_i - c)[\![w']\!]_i - \Delta Q_i w(z_i) = 0 \quad (41)$$

at each of the N vorticity interfaces. Once we write $[\![w']\!]_i = -ik\hat{q}_i$, and substitute for $w(z_i)$ from (40), an eigenvalue problem can be written for the eigenvalue c as

$$A_{ij}\hat{q}_i = c\hat{q}_i \quad \text{with} \quad A_{ij} = U_i\delta_{ij} + \frac{\Delta Q_i}{2k} e^{-k|z_i - z_j|}. \quad (42)$$

This formulation may now be used to investigate solutions to Rayleigh's equation for any general shear flow profile. Note that if a single vorticity interface is present then (41) can be reduced to show the dependence of the vortex sheet strength to the interface displacement $\hat{q}_i = i\Delta Q_i \eta_i / k$, as discussed previously.

To couple the sheared airflow to the surface gravity wave, we use Miles' approximation and let $c = c_0$. We use a normalization condition of $w(0) = 1$ to convert the problem to a nonhomogeneous system of equations. Then, upon solving for the $\hat{q}_i$, we are able to find the growth rate from (16). What is crucial to the success of this method is adequate resolution of the critical layer vorticity field, as shown in Fig. 1. Therefore, the vertical spacing between interfaces must be fine enough to resolve the scale δ_c. This makes the method of solution extremely inefficient, particularly with

regular spacings of z_i. In addition, it is necessary to choose a value of $c = c_0 + ic_i$ with a nonzero imaginary part that can produce a critical layer that is resolved by the interface spacing. To get the correct critical layer thickness in the vorticity field, iteration is therefore needed to adjust c_i from the calculated growth rate. The growth rates found in this way differ from the exact solution (19) and (16) by no more than a fraction of a percent error (Fig. 5).

However, we can instead choose not to resolve the critical layer vorticity field and use the vortex sheet representation found in (32). This is equivalent to extending the minimal model to include vorticity perturbations in the airflow outside of the critical layer. The vertical velocity field can then be written as

$$w(z) = \frac{i}{2}\left(\hat{q}_c e^{-k|z-z_c|} + \sum_{i=0}^{N}{}^{\circ}\, \hat{q}_i e^{-k|z-z_i|}\right), \tag{43}$$

where the circle in the summation indicates that the critical layer interface is not included in the sum. Proceeding as in the minimal model formulation, we substitute $\hat{q}_c = -2\pi\beta_c W_c$, solve for the vertical velocity within the critical layer W_c, and can write

$$w(z) = \frac{i}{2}\sum_{i=0}^{N}{}^{\circ}(\alpha_c e^{-k|z_c-z_i|}e^{-k|z-z_c|} + e^{-k|z-z_i|})\hat{q}_i, \tag{44}$$

where we have defined $\alpha_c \equiv -2\pi\beta_c/(1 + i\pi\beta_c)$. The presence of the additional term (beginning with α_c) represents the reaction of the critical layer interface to the vertical velocity incident on it by the vorticity perturbation at z_i. Applying the jump condition [(41)] at all noncritical layer interfaces and setting $c = c_0$ (with $c_i = 0$) gives the system of equations

$$B_{ij}\hat{q}_i = 0, \tag{45}$$

where

$$B_{ij} = (U_i - c_0)\delta_{ij} - \frac{i\Delta Q_i}{k}(\alpha_c e^{-k|z_c-z_i|}e^{-k|z_j-z_c|} + e^{-k|z_j-z_i|}), \tag{46}$$

which is combined with a normalization condition $w(0) = 1$, that is,

$$\frac{i}{2}\sum_{i=0}^{N}{}^{\circ}(\alpha_c e^{-k|z_c-z_i|}e^{-k|z_c|} + e^{-k|z_i|})\hat{q}_i = 1. \tag{47}$$

This series of (45)–(47) extends the minimal model from the last section to account for vorticity perturbations in the airflow. The minimal model is recovered in the limit of $N \to 1$.

In Fig. 5 we compare growth rate curves obtained from these methods described above to the exact solution using Miles' approximation and the minimal model for the case of $m = 0.0625$. This figure shows first that, when the critical layer is resolved by the interface spacing, the growth rates are accurately calculated and are seen to match the exact solution (i.e., the red dots lie on the thick black curve). Note that an extremely large number of interfaces is required to accurately resolve the critical layer, and this does not represent an efficient numerical solution method. One must therefore be cautious with the use of piecewise profiles, as discussed in Young and Wolfe (2014). Second, Fig. 5 shows that when the critical layer is represented by the vortex sheet in (32), the growth rates rapidly converge to the exact solution as N is increased. This demonstrates also that the critical layer can be parameterized in stability calculations using the vortex sheet representation so that a more efficient numerical solution algorithm can be used.

6. Discussion

a. *Assessing the minimal model*

It is helpful now to consider the relative contribution of the different levels in the airflow to the growth of the surface wave and to use this to understand physically the source of the difference in growth rates between the minimal model and the true growth rates at low k. This is done by using the partial growth rate approach of Carpenter et al. (2010) to split the total growth rate of the surface displacement into its different contributions from each level of the airflow above. We define a partial growth rate profile $\gamma(z)$ that has the property

$$\int_0^\infty \gamma(z)\, dz = \sigma. \tag{48}$$

We can get an expression for γ from a rearrangement of the linearized kinematic condition at the water surface

$$\sigma = \mathrm{Re}\left(\frac{rw_s}{\eta_s}\right) \tag{49}$$

and by realizing that w_s due to the airflow above can be written as

$$w_s = \int_0^\infty q(z)G(z,0)\, dz = -\int_0^\infty U''(z)\eta(z)G(z,0)dz. \tag{50}$$

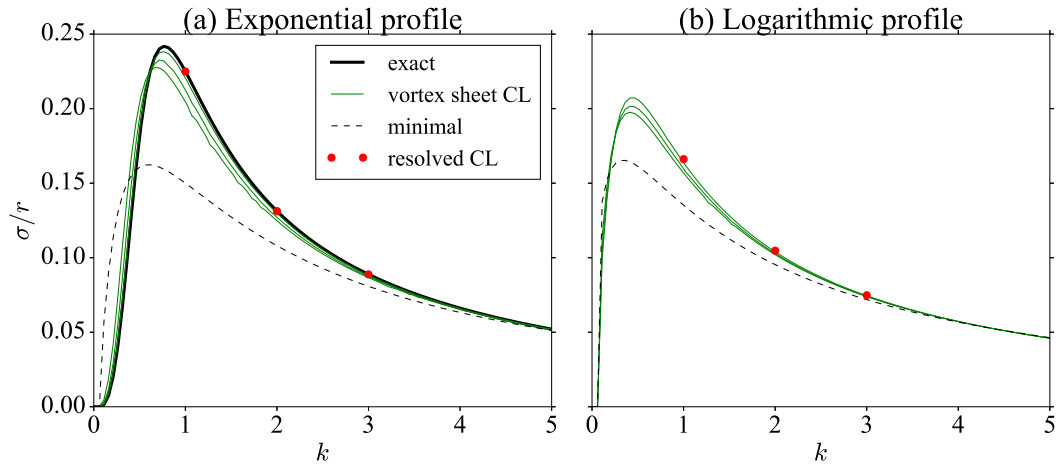

FIG. 5. Comparison of growth rate curves obtained from different methods using both (a) the exponential profile and (b) the classic logarithmic profile $U(z) = \ln(z + 1)$, similar to Morland and Saffman (1993) and Alexakis et al. (2002). The exact solution for the exponential profile from (19) and (16) is found to agree with the method of resolving the critical layer using many vorticity interfaces, as shown by the agreement between the red points and the solid black curve in (a). In this case, the numerical solution (red dots) required $7763 \le N \le 14\,384$ interfaces to resolve the critical layer, corresponding to a resolution of $\Delta z_i = 2 \times 10^{-4}$ and a domain size of $10 z_c$. The thin solid green curves correspond to significantly lower resolutions where $N = 39, 89, 389$, made possible by using the vortex sheet representation of the critical layer. When this representation is used, the growth rate curves quickly approach the exact solution for increasing N in (a) and also approach the numerical results where the critical layer is resolved (red dots, with $7763 \le N \le 14\,384$) for the logarithmic profile in (b). No exact solution is available for the logarithmic profile in (b). In both panels $m = 0.0625$. The velocity and length scales (U_∞, h) in the nondimensionalization of the logarithmic profile are defined through $U_\infty \equiv U_s' h$, where h is the distance below the water surface to the asymptote in U, and U_s' is the profile shear at the water surface. The dimensional profile can be written $U(z) = U_\infty \ln(z/h + 1)$, and the nondimensionalization follows as before from these scales for U_∞, h.

Combining these two expressions and substituting for Green's function gives the desired result,

$$\gamma(z) = r \,\mathrm{Im}\left[\frac{U''(z)\eta(z)e^{-k|z|}}{2\eta_s}\right]. \tag{51}$$

Note that the use of (49) for computing growth rates is not consistent with Miles' approximation.[2]

In Fig. 6 we analyze the case of $m = 0.5$ and $k = 1$, showing the phase and amplitude of the vertical displacements in the airflow relative to the surface wave displacement, $\eta(z)/\eta_s$, both for the full profile (Fig. 6a) and in the region of the critical layer (Figs. 6b,c). The rapid phase change of π across the critical layer is seen in Figs. 6a and 6c, while the amplitude shows a spike centered on the critical height in Fig. 6b. [A full depth plot of $\eta(z)/\eta_s$, is not shown for the z/z_c axis because it consists only of an extremely thin spike at $z/z_c = 1$.] It is the sign of the phase of $\eta(z)/\eta_s$, that sets the sign of γ, separating the profile into regions contributing to growth (negative phase) or decay (positive phase) of the surface wave. This phase relationship is most important in the region of the critical layer, where $|\eta|$ reaches the largest values. This is seen in the rapid decay of $\gamma(z)$ to zero away from the critical layer in Fig. 6d.

The majority of the difference in γ between the minimal and the exact solutions can be attributed to the larger values of $|\eta|$ in the critical layer (a factor of approximately 0.62 versus 0.85 for the phase difference). We propose that the reason for this significant difference is due to the influence of the airflow in the region between the water surface and the critical height that is not accounted for in the minimal model.

To test this idea, we compare $|w(z)|$ profiles generated by the surface wave with and without accounting for disturbances in the airflow vorticity field in Figs. 7a and 7b. In the absence of airflow vorticity perturbations, we can write the vertical velocity induced by the surface wave as $w(z) = e^{-k|z|}$, taking unit amplitude. This will create a vertical displacement of the vorticity gradients in the airflow above, which Fig. 6a shows are largely in phase with the surface displacement. The influence of this region of vorticity perturbation on the w field can be found from

$$w(z) = -\int_0^Z U''(s)\eta(s)G(s,z)\,ds, \tag{52}$$

[2] In this analysis, we include only airflow components and neglect baroclinic vorticity production at the air–water interface.

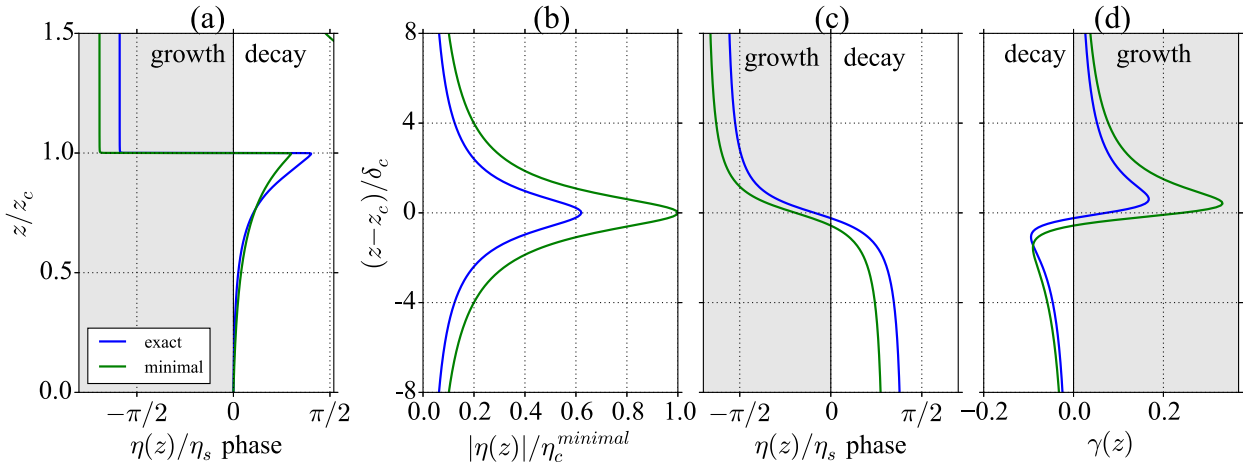

FIG. 6. Comparison of the minimal model with the exact solution: (a) the phase of $\eta(z)/\eta_s$ in the airflow and close ups of the critical layer (b) amplitudes and (c) phase change. In (a) and (c) the gray region with a negative phase provides a contribution to the growth of the surface wave. (d) The partial growth rate profile is shown for the critical layer region. Outside of the critical layer the airflow has a negligible contribution to surface wave growth, and γ is very small. Parameters chosen for these plots are $m = 0.5$, $k = 1$, where disagreement with the minimal model growth rate is large.

where $Z = z_c/2$ is chosen as the upper integration limit, and as a first approximation we take the displacement to be $\eta(z) = e^{-k|z|}/[ik(U-c)]$. The results for low and high k are shown in Figs. 7a and 7b and demonstrate that a significant damping of the w field of the surface wave is to be expected at low k. The physical reason for this damping is illustrated in the sketch in Fig. 7c; in-phase displacements of vorticity above the surface wave contribute to an opposite w field as the surface displacement, and this leads to a reduced w incident on the critical layer.

This analysis demonstrates that the airflow vorticity can lead to reduced vertical velocities in the critical layer from the surface wave influence and therefore reduced growth rates than predicted by the minimal model. However, it can also be the case that the minimal model underpredicts the growth rate, as exemplified at $m = 0.0625$, $k = 1$ (Fig. 4). Using a similar analysis as above, it can be shown that the displacements in the critical layer are larger in this case when the airflow vorticity perturbations are accounted for. This is the opposite situation as just described for $m = 0.5$ and arises because of the penetration of the surface wave vertical velocity *above* the critical layer. Since the surface wave vertical velocity decays over the length scale k^{-1}, the critical layer is relatively close to

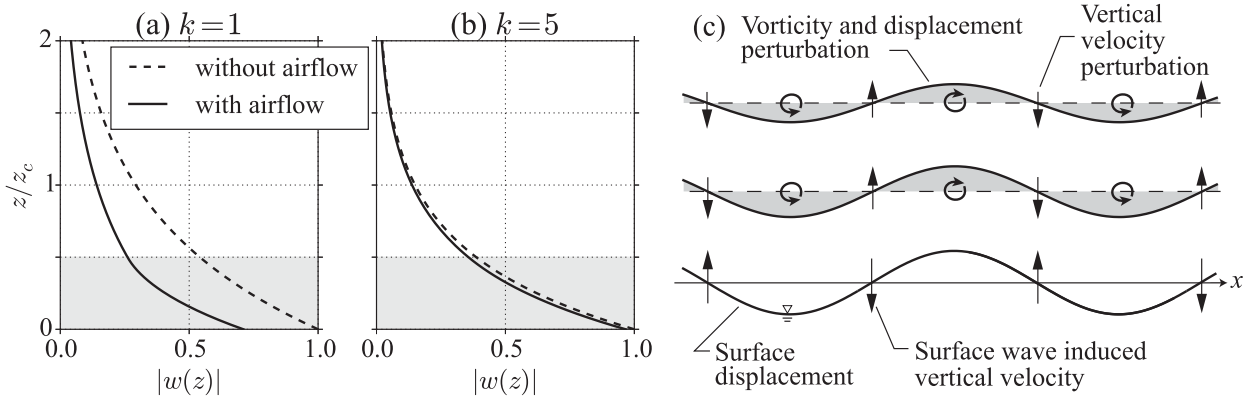

FIG. 7. Vertical velocity amplitudes in the airflow with and without accounting for perturbations in the vorticity field above the surface wave. Profiles are shown at k = (a) 1 and (b) 5. Parameters chosen for these plots are $m = 0.5$ and an upper integration limit of $Z = z_c/2$ (shown in gray). (c) Sketch of the mechanism by which airflow perturbations damp the w field of the surface wave.

the surface wave at $m = 0.0625$ with $kz_c = 0.29$, whereas for $m = 0.5$ the surface wave is distant with $kz_c = 1.23$. Therefore, the surface wave excites displacements that are not directly in phase with itself, leading in this case to a larger vertical velocity and vorticity inside the critical layer.

In summary, we can attribute the growth of the surface wave displacement to the vorticity perturbations within the critical layer. However, this critical layer vorticity amplitude and phase is dependent on the vertical velocity incident on the critical layer W_c. To correctly capture this W_c at low k, it is necessary to include the effects of vorticity perturbations in the airflow that lie outside of the critical layer. There is an indirect effect of the airflow perturbations outside of the critical layer that contribute to the incident vertical velocity W_c. This is a result of the nonlocal nature of the vertical velocity, which is dependent on an integral over the entire vorticity field. Since the perturbation vorticity comes from the displacement of a continuous U'', the vertical velocity at a given height has its source throughout the profile. The vorticity, in contrast, is local since it is determined entirely by local displacements of the background profile.

b. *Relation to wave interaction theory*

The present analysis represents an extension of previous applications of WIT for understanding the mechanisms of instability in stratified shear flows (e.g., Baines and Mitsudera 1994; Heifetz et al. 2006; Carpenter et al. 2010; Rabinovich et al. 2011). This arises from our new treatment of the critical layer as another type of ''interface'' that is able to interact with the other waves present in the background profiles. Although this idea has been used qualitatively by Rabinovich et al. (2011) and Heifetz et al. (2015), the present study is the first to develop a quantitative description of critical layer wave interactions.

The application of WIT involves two fundamental conditions that must be satisfied for instability to occur between two interacting interfacial waves: (i) a ''phase locking'' of the waves must occur so they are stationary with respect to each other and (ii) they must be in a configuration that allows mutual growth (Redekopp 2001; Carpenter et al. 2013). In the case of the wind-wave instability, the first condition is satisfied as long as the critical layer exists, that is, when the gravity wave phase speed lies within the range of the background velocity profile, $c_0 < U_\infty$ in dimensional units. For a background flow that is in the positive x direction, this therefore excludes an interaction between the leftwards propagating gravity wave. Additionally, the second condition is nearly always satisfied since the critical layer produces a vertical velocity field that is $\pi/2$ out of phase with the vertical velocity incident on it. An exception, which is likely not found in the boundary layer profiles commonly observed in the ocean–atmosphere boundary layer, is if the background flow curvature at the critical height $U_c'' > 0$. In this case, the critical layer would produce a vorticity sheet strength of the opposite sense and lead to a $\pi/2$ phase shift that would cause a decay of the surface wave (simply reverse the critical layer vertical velocity arrows in Fig. 3). Carpenter et al. (2013) discuss how these two conditions correspond to the necessary conditions for instability of Rayleigh and Fjørtoft.

Despite the natural extension of WIT to critical layers, the critical layer interface is not like other interfaces (e.g., density or vorticity interfaces) because it does not support wave motion when in isolation (i.e., in the absence of interaction). In contrast, the critical layer interface simply chooses the level of the background flow such that it moves at the speed of the surface gravity wave forcing it. Therefore, the region of wavenumber space that allows for phase locking corresponds to the wavenumbers that have phase speeds within the range of the background flow profile. This is a consequence of Miles' approximation that does not account for the altering of the phase speed of the surface gravity wave by the airflow in the determination of growth rates at order r. In the Boussinesq case of internal wave interaction with a critical layer, this phase speed alteration must be accounted for.

7. Summary

In this study, we have used the framework of wave interaction theory for describing the physical mechanism by which a sheared airflow generates the growth of surface gravity waves. This is done by first formulating an approximate analytical model for the structure of the vertical displacement, vorticity, and vertical velocity fields within the narrow critical layer region. The basis for this model is the realization that the vertical velocity varies over a vertical length scale that is comparable to the disturbance wavelength, whereas the displacement and vorticity varies over a much smaller length scale, $\delta_c \ll k^{-1}$. The resulting displacement and vorticity structure of the critical layer can then be understood as arising from the competition between horizontal advection and unsteady growth of the displacement field caused by an incident vertical velocity. This vertical velocity originates from the surface gravity wave, as well as from perturbations of the airflow vorticity.

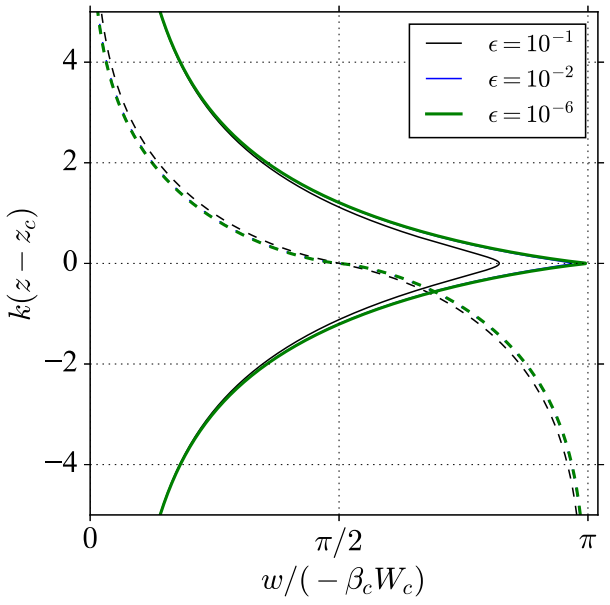

FIG. A1. The vertical velocity structure at the critical layer due to the incident vertical velocity W_c, with an infinite region of integration, that is, $K(kz, i\varepsilon, \pm\infty)$. The solid lines denote the amplitude, and the dashed lines denote the phase. Three values of ε are plotted to show that an asymptotic form is quickly approached for small ε. The blue curve for $\varepsilon = 10^{-2}$ is indistinguishable from that for $\varepsilon = 10^{-6}$.

The localized nature of the critical layer lends itself naturally to an interfacial vortex sheet representation so that a minimal two-wave interaction model can be formulated as in wave interaction theory. The resulting unstable interaction has been found to capture the essence of the wind-wave instability. However, differences between the minimal model and the exact solution are present at low wavenumbers close to maximum growth, and these are demonstrated to be the result of neglecting perturbations in the airflow that contribute to the vertical velocity incident on the critical layer.

Although the aim of the present study has been to develop physical intuition through a wave interaction interpretation of the wind-wave instability, the concepts applied to describe the critical layer are more general than this specific problem. In future work, we shall apply these concepts to density stratified critical layers that arise in the instability of more general continuously stratified shear flows.

Acknowledgments. We would like to acknowledge helpful discussions with Marc Buckley. Partial funding has been provided by the PACES II programme of the Helmholtz Association (JRC). This paper is also a contribution to the Collaborative Research Centre TRR 181 "Energy Transfer in Atmosphere and Ocean" funded by the German Research Foundation.

APPENDIX

Vertical Velocity for Large Integration Limits

A second case, where the limits of integration of (26) are taken to be very large, is also of interest. This limit $y_c^{\pm} \to \pm\infty$ is equivalent to assuming that the velocity profile has a constant U'', U', and W_c that are fixed at the critical layer values. The resulting w is shown in Fig. A1 and has qualitatively the same structure as the η and q fields, with a maximum amplitude at z_c and a phase change of π radians. However, the variation in w that occurs across the critical layer has the characteristic length scale of k^{-1} and is why we choose $k(z - z_c)$ for the vertical coordinate, rather than $(z - z_c)/\delta_c$ as for the structure of the η and q fields. In addition, w is seen to approach an asymptotic form for sufficiently small values of the dimensionless parameter ε that is an excellent approximation for wind waves. This is equivalent to the limit of small critical layer thickness compared to the disturbance wavelength, since $\varepsilon = k\delta_c \mathrm{sign}(U_c')$. However, the region over which the phase change in w occurs in Fig. A1 is similar to the dimensionless critical layer height kz_c. This suggests that it is not an accurate representation of the local critical layer response, considering the large changes in U'', U', and W_c that can occur over the distance kz_c. We therefore have used the local representation in section 3.

REFERENCES

Alexakis, A., Y. Young, and R. Rosner, 2002: Shear instability of fluid interfaces: Stability analysis. *Phys. Rev. E*, **65**, 026313, doi:10.1103/PhysRevE.65.026313.

——, ——, and ——, 2004a: Weakly nonlinear analysis of wind-driven gravity waves. *J. Fluid Mech.*, **503**, 171–200, doi:10.1017/S0022112003007699.

——, and Coauthors, 2004b: On the nonlinear evolution of wind-driven gravity waves. *Phys. Fluids*, **16**, 3256, doi:10.1063/1.1771695.

Baines, P., and H. Mitsudera, 1994: On the mechanism of shear flow instabilities. *J. Fluid Mech.*, **276**, 327–342, doi:10.1017/S0022112094002582.

Belcher, S., and J. Hunt, 1993: Turbulent shear flow over slowly moving waves. *J. Fluid Mech.*, **251**, 109–148, doi:10.1017/S0022112093003350.

——, and ——, 1998: Turbulent flow over hills and waves. *Annu. Rev. Fluid Mech.*, **30**, 507–538, doi:10.1146/annurev.fluid.30.1.507.

Buckley, M., and F. Veron, 2016: Structure of the airflow above surface waves. *J. Phys. Oceanogr.*, **46**, 1377–1397, doi:10.1175/JPO-D-15-0135.1.

Bühler, O., 2009: *Waves and Mean Flows.* Cambridge University Press, 370 pp.

Carpenter, J., N. Balmforth, and G. Lawrence, 2010: Identifying unstable modes in stratified shear layers. *Phys. Fluids*, **22**, 054104, doi:10.1063/1.3379845.

——, E. Tedford, E. Heifetz, and G. Lawrence, 2013: Instability in stratified shear flow: Review of a physical interpretation based on interacting waves. *Appl. Mech. Rev.*, **64**, 060801, doi:10.1115/1.4007909.

Caulfield, C., 1994: Multiple linear instability of layered stratified shear flow. *J. Fluid Mech.*, **258**, 255–285, doi:10.1017/S0022112094003320.

Drazin, P., and W. Reid, 1982: *Hydrodynamic Stability*. Cambridge University Press, 682 pp.

Grare, L., L. Lenain, and W. Melville, 2013: Wave-coherent airflow and critical layers over ocean waves. *J. Phys. Oceanogr.*, **43**, 2156–2172, doi:10.1175/JPO-D-13-056.1.

Harnik, N., E. Heifetz, O. Umurhan, and F. Lott, 2008: A buoyancy-vorticity wave interaction approach to stratified shear flow. *J. Atmos. Sci.*, **65**, 2615–2630, doi:10.1175/2007JAS2610.1.

Heifetz, E., and J. Mak, 2015: Stratified shear flow instabilities in the non-Boussinesq regime. *Phys. Fluids*, **27**, 086601, doi:10.1063/1.4928738.

——, Y. Reuveni, A. Gelfgat, E. Kit, and J. Methven, 2006: Counterpropagating Rossby wave perspective on Kelvin Helmholtz instability as a limiting case of a Rayleigh shear layer with zero width. *Phys. Fluids*, **18**, 018101, doi:10.1063/1.2166450.

——, J. Mak, J. Nycander, and O. Umurhan, 2015: Interacting vorticity waves as an instability mechanism for MHD shear instabilities. *J. Fluid Mech.*, **767**, 199–225, doi:10.1017/jfm.2015.47.

Hristov, T. S., S. D. Miller, and C. A. Friehe, 2003: Dynamical coupling of wind and ocean waves through wave-induced air flow. *Nature*, **422**, 55–58, doi:10.1038/nature01382.

Hughes, T., and W. Reid, 1965: On the stability of the asymptotic suction boundary-layer profile. *J. Fluid Mech.*, **23**, 715–735, doi:10.1017/S0022112065001647.

Janssen, P., 2004: *The Interaction of Ocean Waves and Wind.* Cambridge University Press, 312 pp.

Jeffreys, H., 1925: On the formation of water waves by wind. *Proc. Roy. Soc. London*, **A107**, 189–206, doi:10.1098/rspa.1925.0015.

Kelvin, W., 1871: Hydrokinetic solutions and observations. *Philos. Mag.*, **42**, 362–377.

Kinsman, B., 1965: *Wind Waves: Their Generation and Propagation on the Ocean Surface.* Prentice-Hall, 676 pp.

Lighthill, M. J., 1962: Physical interpretation of the mathematical theory of wave generation by wind. *J. Fluid Mech.*, **14**, 385–398, doi:10.1017/S0022112062001305.

Maslowe, S. A., 1986: Critical layers in shear flows. *Annu. Rev. Fluid Mech.*, **18**, 405–432, doi:10.1146/annurev.fl.18.010186.002201.

Miles, J., 1957: On the generation of surface waves by shear flows. *J. Fluid Mech.*, **3**, 185–204, doi:10.1017/S0022112057000567.

Morland, L., and P. Saffman, 1993: Effect of wind profile on the instability of wind blowing over water. *J. Fluid Mech.*, **252**, 383–398, doi:10.1017/S0022112093003805.

Phillips, O., 1957: On the generation of waves by a turbulent wind. *J. Fluid Mech.*, **2**, 417–445, doi:10.1017/S0022112057000233.

Rabinovich, A., O. Umurhan, N. Harnik, F. Lott, and E. Heifetz, 2011: Vorticity inversion and action-at-a-distance instability in stably stratified shear flow. *J. Fluid Mech.*, **670**, 301–325, doi:10.1017/S002211201000529X.

Redekopp, L., 2001: Elements of instability theory for environmental flows. *Environmental Stratified Flows*, Kluwer, 223–281.

Sullivan, P., and J. McWilliams, 2010: Dynamics of winds and currents coupled to surface waves. *Annu. Rev. Fluid Mech.*, **42**, 19–42, doi:10.1146/annurev-fluid-121108-145541.

Young, W., and C. Wolfe, 2014: Generation of surface waves by shear-flow instability. *J. Fluid Mech.*, **739**, 276–307, doi:10.1017/jfm.2013.617.